Nucleation and dynamics of magnetic vortices under spin-polarized current

Yoshinobu Nakatani
Department of Computer Science, University of Electro-Communications, Chofu, Tokyo 182-8585, Japan

Junya Shibata
Kanagawa Institute of Technology, 1030 Shimo-Ogino, Atsugi, Kanagawa 243-0292, Japan

Gen Tatara
Department of Physics, Tokyo Metropolitan University, Hachioji, Tokyo 192-0397, Japan
and PRESTO, JST, 4-1-8 Honcho Kawaguchi, Saitama 332–0012, Japan

Hiroshi Kohno
Graduate School of Engineering Science, Osaka University, Toyonaka, Osaka 560-8531, Japan

André Thiaville and Jacques Miltat
Laboratoire de Physique des Solides, CNRS, Université Paris-Sud, Bâtiment 510, 91405 Orsay Cedex, France
(Received 6 October 2007; published 30 January 2008)

Spin-polarized current in a ferromagnet is known to lead to the instability of the uniformly magnetized state. In this paper, it is demonstrated by micromagnetic simulations that, in films or wide wires, the above instability is followed by the formation of magnetic vortices. Subsequent magnetization dynamics is also studied in terms of vortices, which includes pair dynamics and pair annihilation. Using a simple analytical model that considers the vortices as points, the dynamics of two interacting vortices under the current is classified according to their vorticity and polarity. This explains well the essential features of the simulation results.

DOI: 10.1103/PhysRevB.77.014439 PACS number(s): 75.70.Kw, 72.25.Ba, 85.75.−d

I. INTRODUCTION

Vortices are topological objects playing an essential role in various phenomena in nature. In the atmosphere, formation of large-scale vortices such as low pressure and typhoon crucially affects climate and our everyday life. At the nanoscale, tiny vortices in magnets with a core of typical size ~10 nm govern magnetization dynamics.

Spin manipulation in magnetic nanostructures is becoming highly important for developing high performance magnetic memories with novel architecture. Particularly, use of current instead of magnetic field turns out to be quite advantageous from the viewpoint of scalability, besides its interest in fundamental physics.

The most effective driving mechanism in nanoscale systems is the spin-transfer effect proposed for domain-wall motion[1] and magnetization reversal in pillar systems.[2,3] This effect is due to the transfer of electron spin angular momentum to magnetization and can, in principle, drive any slowly varying magnetization pattern to a velocity $v_s \equiv (\gamma\hbar/2eM_s)j_s$. Here, j_s, M_s, and $\gamma = g\mu_B/\hbar$ are the spin-current density (associated with the usual electric current in ferromagnets), the saturation magnetization, and the gyromagnetic constant, respectively (μ_B and g are Bohr magneton and g factor, respectively). Experimentally, domain-wall motion sets in above a rather high threshold current density of $\sim 10^9$ A/m^2 in magnetic semiconductors[4,5] and $\sim 10^{12}$ A/m^2 in metals.[6–11] Qualitative behaviors seem to agree with spin-transfer theories,[1,12–16] but quantitative interpretation is still controversial.

Another important aspect of the spin-transfer effect is that it can induce topologically nontrivial spin textures and lead to an instability of the uniformly magnetized state.[17–20] This instability was shown to trigger domain-wall formation in a narrow wire if the current is sufficiently high.[20] With this domain formation, combined with wall motion by spin transfer, one can implement, in principle, a domain-wall memory where the full cycle of writing and erasing is carried out directly by current.

Vortices are known to affect magnetization dynamics in thin films.[21–23] Actually, a domain wall in a wide nanowire contains a vortex as a stable structure, and its dynamics is determined by that of the vortex.[9,13,24] Current-induced motion of a vortex in a single nanodot has also been recently investigated, both experimentally[24–28] and theoretically.[29,30]

In this paper, we demonstrate by micromagnetic simulations that the instability of the uniformly magnetized state in wide wires and films leads to the formation of vortices. A detailed description of vortex-pair creation, dynamics, and annihilation under spin current is obtained by micromagnetic simulations and analytical calculations. Domain walls are shown to be created via individual annihilations of vortices across the sample edges. Vortices under spin current do not suffer from intrinsic pinning,[29] in contrast to domain walls,[12,13] and so would be useful for efficient memory devices operated at low current.

A magnetic vortex, in general, is a topological configuration illustrated in Fig. 1. It is characterized by two integers. The first one is the vorticity, $q = \pm 1, \pm 2, \ldots$, which is the winding number of the in-plane magnetization component. Low energy magnetization dynamics is described by the simplest configurations with $q = \pm 1$. The second one is the polarity, $p = \pm 1$, or equivalently written as $p = \uparrow, \downarrow$, which specifies the direction of the out-of-plane component at the

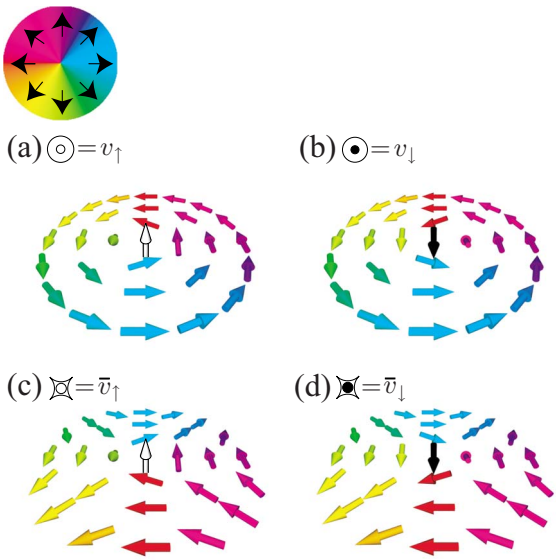

FIG. 1. (Color online) Schematic of magnetization pattern of magnetic vortices. They are characterized by vorticity q and polarity p: (a) $(q,p)=(1,1)$, (b) $(q,p)=(1,-1)$, (c) $(q,p)=(-1,1)$, and (d) $(q,p)=(-1,-1)$. At the center, the magnetization rises out of the plane and points upward ($p=\uparrow$ or 1) or downward ($p=\downarrow$ or -1). The color represents the in-plane magnetization direction as defined in the top panel; the out-of-plane component is expressed by white ($m_z>0$) or black ($m_z<0$). Structures (a) and (b) are called vortices, and (c) and (d) antivortices.

core of the configuration. In a more precise sense, we call the configuration with $q=1$ a vortex and that with $q=-1$ an antivortex and denote them as v and $\bar{v}$, respectively. The core polarity will also be specified by the notations v_p and $\bar{v}_p$, such as $v_\uparrow$.

II. SIMULATION RESULTS

Micromagnetic simulations have been performed according to the Landau-Lifshitz-Gilbert equation

$$\dot{\boldsymbol{m}} = \gamma_0 \boldsymbol{H}_{\text{eff}} \times \boldsymbol{m} + \alpha \boldsymbol{m} \times \dot{\boldsymbol{m}} - (\boldsymbol{v}_s \cdot \nabla)\boldsymbol{m}, \qquad (1)$$

describing the dynamics of magnetization vector $\boldsymbol{M}$ or its direction $\boldsymbol{m}=\boldsymbol{M}/M_s$. The first two terms on the right-hand side are the usual micromagnetic torques (with $\gamma_0=\mu_0|\gamma|$), and the effective field $\boldsymbol{H}_{\text{eff}}$ includes exchange and demagnetizing fields. (We consider in this paper a material with no magnetocrystalline anisotropy.) The second term is the Gilbert damping, with α being the damping constant. The last term represents the spin-transfer torque.[31]

The micromagnetic calculation program used in the simulation is based on the previously developed code.[13,15,32–35] The sample is divided into identical rectangular prisms with the size of $2.5\times2.5\times5$ nm^3. The calculation region is 2.55 μm in length, 80 nm in width, and 5 nm in thickness. Free boundary conditions are adopted on the wire lateral surfaces, and fixed boundary conditions applied to both ends in the wire direction. The magnetic moments in the initial state are aligned along the wire direction ($+x$ direction). A uniform

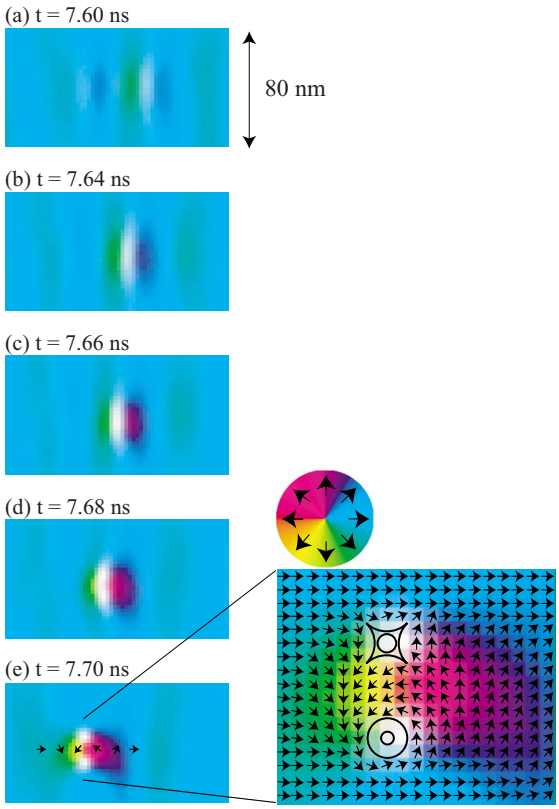

FIG. 2. (Color online) Snapshot illustrations of the nucleation process of a vortex-antivortex (v-$\bar{v}$) pair induced by spin current in a nanowire of 80 nm width, 5 nm thickness, and 2.55 μm length for $j_s=1.7\times10^{13}$ A/m^2 ($v_s=1200$ m/s) and $\alpha=0.03$. Illustrations are focused on the nucleation region. The magnetization direction is represented by colors, as explained in Fig. 1. (a) Ripples of precessional spin waves. [(b)–(d)] Growth of the precession amplitude. (e) Nucleation of a v-$\bar{v}$ pair (white dots). In-plane magnetization direction is indicated also by arrows. The close-up shows magnetization distribution around the v-$\bar{v}$ pair. The nucleated v and $\bar{v}$ have the same polarity ($p=1$).

current is applied in the direction of the magnetic moments (the direction of the electron flow is opposite). The intensity of the current is maximum and constant in the center 1/3 area and falls linearly to zero on both ends to avoid boundary effects. Thermal noise of $T=4$ K is applied in order to accelerate the instability.[36,37] The nucleation time of vortices was indeed seen to decrease in the presence of thermal noise, but the threshold j_s^{th} (described below) did not change.

The simulation results are shown in Figs. 2–4 for $j_s=1.7\times10^{13}$ A/m^2 (which corresponds to $v_s=1200$ m/s) and $\alpha=0.03$. The phenomena described in the following have been observed for j_s exceeding a certain threshold, j_s^{th}, which is $j_s^{\text{th}}=1.4\times10^{13}$ A/m^2 in our simulations. This threshold is weakly dependent on α, as expected from previous works,[19,20] and is reduced for thicker samples. In simple terms, the excitation of spin waves is driven by the linear shift of their energy under spin-polarized current.[17,18]

The first signature indicating the instability of the uniform state appears as ripples of coherent spin waves. This is a precessional wave motion of magnetization around the mag-

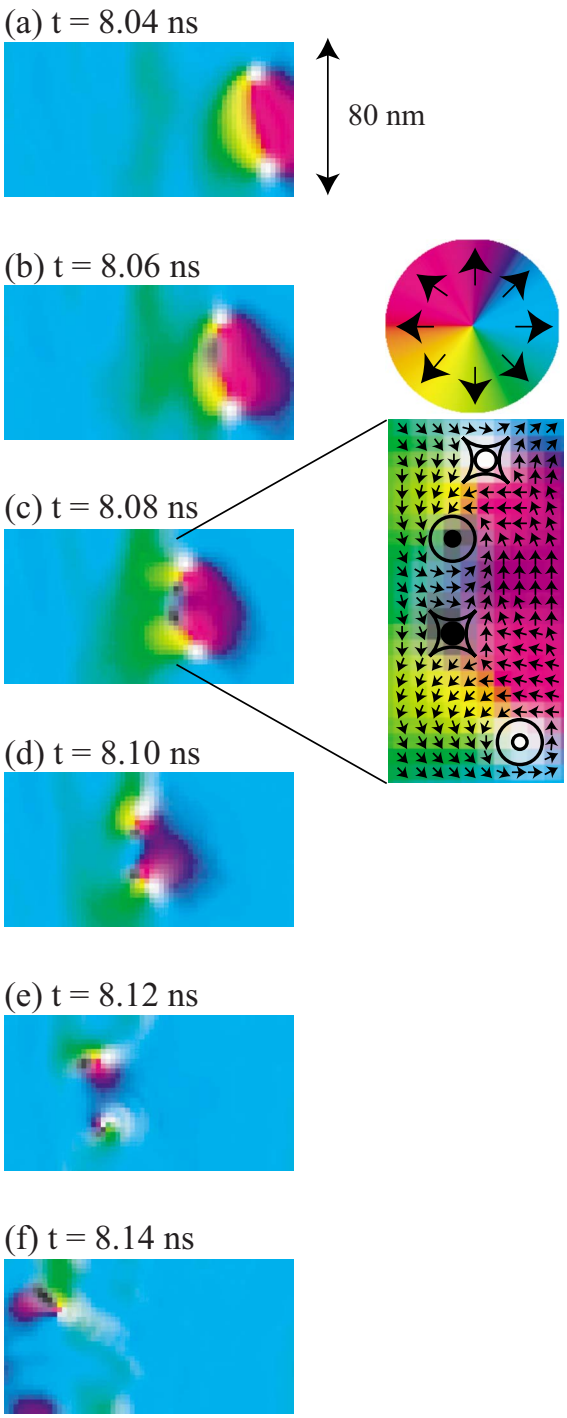

FIG. 3. (Color online) Snapshot illustrations of motion and annihilation of a vortex-antivortex (v-$\bar{v}$) pair under spin current in the same nanowire, as in Fig. 2. Illustrations are focused on the region of interest. [(a) and (b)] A v-$\bar{v}$ pair with same polarity (white dots; $p=1$) moving along the wire. (c) Nucleation of another v-$\bar{v}$ pair (black dots; $p=-1$) having opposite polarity with that of the existing pair. The close-up shows magnetization distribution around the two v-$\bar{v}$ pairs. [(d) and (e)] Mutual rotation, like multiple star, of v and $\bar{v}$ having opposite polarities in each pair [see Fig. 5(d)]. (f) Pair annihilations followed by large-amplitude spin-wave emission.

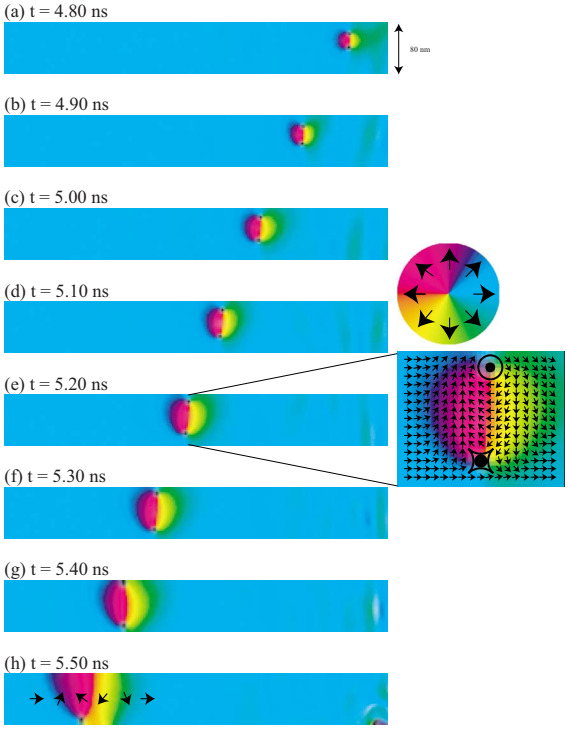

FIG. 4. (Color online) Snapshot illustrations of pair creation of domain walls under spin current in the same nanowire, as in Fig. 2. [(a)–(g)] A v-$\bar{v}$ pair of vortices with same polarity ($p=-1$) moves along the wire and increases its separation [see Fig. 5(c2)]. A close-up for (e) shows the magnetic domain structure inside the v-$\bar{v}$ pair. (h) A pair of domain walls is left after the v and $\bar{v}$ disappear through different lateral edges of the wire.

netic easy axis (i.e., wire direction), whose amplitude is initially small. A snapshot is shown in Fig. 2(a), where the wavelength is approximately $\lambda_0=300$ nm. This ripple pattern then flows in the direction of electron flow due to the spin-transfer mechanism, but the velocity ($\sim$300 m/s) is much lower than v_s expected in the full spin-transfer case. The amplitude of spin-wave precession grows gradually [Figs. 2(a)–2(d)] and the ripple pattern starts to fluctuate. At some crest of the ripple, the out-of-plane component develops significantly and the magnetization points perpendicular to the plane locally. This region with $m_z=1$ (or -1), which is string shaped, eventually splits into two vortices (precisely speaking, one vortex v and one antivortex $\bar{v}$), as seen in Fig. 2(e). This is the v-$\bar{v}$ pair creation induced by spin current. The nucleated vortex and the antivortex have the same polarity, as seen from Fig. 2(e) as white dots, and are connected by two domain walls [yellow and dark blue in Fig. 2(e)] with a reversed domain in between [the red region in Fig. 2(e)]. This polarity is inherited from the out-of-plane component that has grown from the ripple.

The pair then flows along the current (Fig. 3) at the speed of v_s,[29] much faster than the ripple pattern. Calculations show that the pair separates under spin-transfer torque (as will be explained later, this occurs because polarities are identical in the pair). The ultimate fate of the nucleated vortices is thus either of the following: (i) the v_p-$\bar{v}_p$ pair is annihilated with another $v_{\bar{p}}$-$\bar{v}_{\bar{p}}$ pair with opposite polarity or

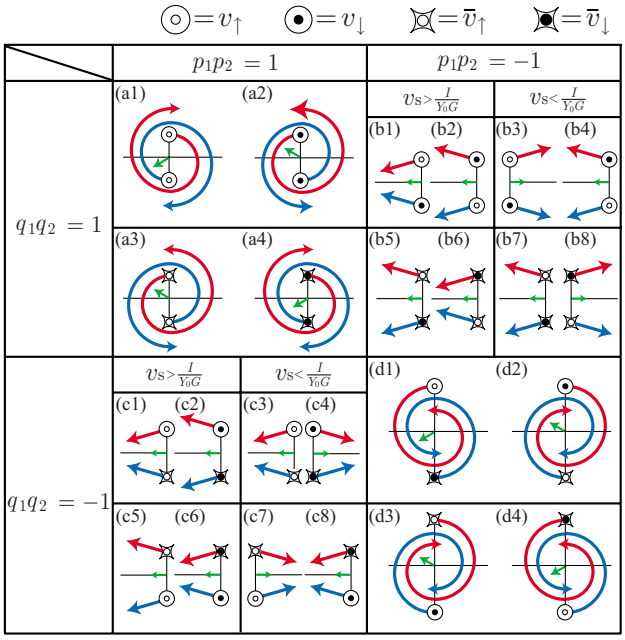

FIG. 5. (Color online) Classification of the motion of two vortices under spin current. The green arrows stand for the initial velocity of the center of mass of two vortices. Vortices and antivortices are represented by a circle with white dot ($v_\uparrow$;$p=q=1$), a circle with black dot ($v_\downarrow$;$-p=q=1$), an asteroid with white dot ($\bar{v}_\uparrow$;$p=-q=1$), and an asteroid with black dot ($\bar{v}_\downarrow$;$p=q=-1$). For $p_1q_1p_2q_2=1$, two vortices with same polarities (a) or vortex and antivortex with mutually opposite polarities (d) exhibit a circular relative motion. For $p_1q_1p_2q_2=-1$, two vortices with mutually opposite polarities (b) or vortex and antivortex with same polarities (c) exhibit a rectilinear motion. The pair annihilation process of Figs. 3(d)–3(f) corresponds to case (d). The v-$\bar{v}$ pair creation of Fig. 2 as well as the domain-wall creation of Fig. 4 correspond to the two cases (c2) and (c5).

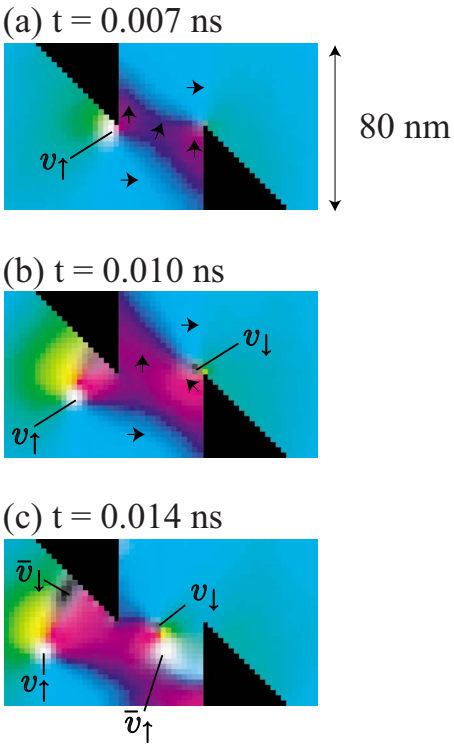

FIG. 6. (Color online) Snapshot of illustrations of the vortex creation process in a nanowire with notches at lower spin-current density $j_s=5.6\times10^{12}$ A/m^2. The sample size is the same as in Fig. 2. Illustrations are focused on the region of interest. (a) A vortex, $v_\uparrow$, is created at the cusp of the upper notch and 90° walls appear between the notches. (b) Another vortex, $v_\downarrow$, is subsequently created at the cusp of the lower notch and the 90° walls are developed. (c) After each vortex is split off from the notch, an antivortex ($\bar{v}_\downarrow$ at the upper notch and $\bar{v}_\uparrow$ at the lower notch) with polarity opposite to the previous vortex, respectively, appears at the edge of each notch. The domain walls then flow away along the wire.

(ii) each vortex (and antivortex) is annihilated at the wire edges.

The first case (i) is shown in Fig. 3. The white stretched string is broken by the nucleation of another v-$\bar{v}$ pair. The newly created v-$\bar{v}$ pair has opposite polarity with that of the existing pair as seen as black spots in Fig. 3(c). The four vortices then recombine into two v-$\bar{v}$ pairs, $v_\uparrow$-$\bar{v}_\downarrow$ and $v_\downarrow$-$\bar{v}_\uparrow$, with zero net polarity in each pair and with strings of reduced length. Having opposite polarities, the v and $\bar{v}$ in the new pair rotate around each other like a multiple star [Figs. 3(d) and 3(e)]. After a few rotations, they annihilate together and the released energy is emitted as spin waves [Fig. 3(f)], as seen already in several calculations[38,39] and experimentally.[40] Note that this process is topologically forbidden, so that it involves a Bloch point.[41] The energy released corresponds to the concentration of exchange energy as the pair is squeezed. This is the pair annihilation of v and $\bar{v}$ having opposite polarities.

The second case (ii) is shown in Fig. 4. When a vortex and an antivortex reach mutually opposite sides of the wire, they can annihilate out of the sample [Fig. 4(g)], leaving behind a stringlike region of opposite domain or a pair of winding transverse domain walls [Fig. 4(h)]. This process gives an alternative path to the current-induced domain-wall formation, which has been considered in thin wires where variation in the transverse direction can be neglected.[20] It will be dominant in wide wires.

These results can be summarized as the following rules for the pair creation and annihilation. A vortex and an antivortex created in pair in the bulk have the same polarity, whereas the pair compression and eventual annihilation under spin-transfer torque is possible only between those with opposite polarity.

Because we put a very large current for vortex nucleation, the effect of the Œrsted field may not be ignored. However, the profile of the current assumed in these simulations has a nonzero div J, so that it is not experimentally realistic and therefore no meaningful field can be computed from it. In order to solve these two questions, we have also performed simulations with a realistic structure for the sample and leads that produces a similar current distribution. This sample structure incorporates two current leads, the left one on top of the sample and the right one below, the length, width, and thickness of the leads being 1/3 of the sample length, the sample width, and 75 nm, respectively. For this structure, we

calculated the nonuniform current distribution and the distribution of the associated Œrsted field. The micromagnetic simulation results with this distribution of current and Oersted field show that the change of the threshold current for vortex nucleation is minor (the threshold current velocity decreased only by 30 m/s). Thus, for the physics studied here, the simplistic current distribution assumed throughout this paper is sufficient.

III. ANALYSIS OF VORTEX-PAIR DYNAMICS

To gain some insight into the vortex dynamics, we focus here on the position of the vortex center and study the motion of a pair of vortices under the spin current with a simple analytical model that considers the vortex and antivortex as points.

The energy of a vortex-antivortex pair contains several contributions. Exchange energy has been considered first.[21] It contains a long-range part that derives from the in-plane magnetization components but also a short-range part that arises when the cores overlap. The short-range part is often neglected as the point vortex model applies only at large separations; it expresses the topological obstruction to pair annihilation. Magnetostatic interactions are also present. Again, a long-range interaction exists due to the modification of the magnetization in-plane component. It is, however, quite complex to evaluate as it requires the full magnetization distribution, in principle (approximate expressions have been devised for finite samples by assuming a magnetostatic charge distribution[42]). A short-range magnetostatic interaction exists similarly, due to the interaction of the dipole moments represented by the cores. All these interaction terms are taken into account in the numerical micromagnetic simulations. We develop below an analytic calculation of the pair dynamics in the regime when cores are far apart, so that the short-range interaction terms are not considered. In a first step, we neglect the long-range magnetostatic interaction between the vortex and antivortex. This already allows understanding the numerical results.

Let the position, polarity, and vorticity of each vortex $(i=1,2)$ be $\boldsymbol{X}_i$, p_i, and q_i, respectively. The equations of motion for $\boldsymbol{X}_i$'s are given by[15,21,29,30,45]

$$p_i q_i \boldsymbol{G} \times (\dot{\boldsymbol{X}}_i - \boldsymbol{v}_s) + \alpha D \dot{\boldsymbol{X}}_i = (-1)^{i-1} q_1 q_2 I \frac{\boldsymbol{X}_1 - \boldsymbol{X}_2}{|\boldsymbol{X}_1 - \boldsymbol{X}_2|^2}, \quad (2)$$

where $\boldsymbol{G}=(2\pi L \mu_0 M_s/\gamma_0)\hat{z}$ with L being the thickness of the wire. The first term on the left-hand side consists of the gyroforce $(\propto \boldsymbol{X}_i)$ and the force from the spin current $(\propto \boldsymbol{v}_s)$.[15,29] The vector $p_i q_i \boldsymbol{G}$ is known as a gyrovector. The second term is the damping force, where α is the Gilbert damping parameter and D is a dissipation matrix element.[21] The right-hand side represents the far field exchange interaction between the two vortices $U_{\text{int}}=-q_1 q_2 I \ln(|\boldsymbol{X}_1-\boldsymbol{X}_2|/\delta)$, where $I=AL$ with A the micromagnetic exchange energy constant and δ is the size of the vortex core. It is attractive for $q_1 q_2=-1$ and repulsive for $q_1 q_2=1$.[21]

For a special case of $\alpha=0$ and $\boldsymbol{V}_s=\boldsymbol{0}$, Eq. (2) leads to $\dot{\boldsymbol{X}}_1=-(p_1 q_1 p_2 q_2)\dot{\boldsymbol{X}}_2$. Thus, two types of motion are distinguished by $p_1 q_1 = \pm p_2 q_2$. For $p_1 q_1 = p_2 q_2$ $(\dot{\boldsymbol{X}}_1=-\dot{\boldsymbol{X}}_2)$, the center of mass is at rest. Due to the central force [right-hand side of Eq. (2)] between the two vortices, they exhibit a circular relative motion. On the other hand, for $p_1 q_1 = -p_2 q_2$ $(\dot{\boldsymbol{X}}_1 = \dot{\boldsymbol{X}}_2)$, the two vortices move together and exhibit a rectilinear motion.

Let us now examine the solution of Eq. (2) for finite $\boldsymbol{V}_s=(-v_s,0)$ and finite but small α. The initial condition is taken as $X_1(0)=X_2(0)=0$, $Y_1(0)=-Y_2(0)=Y_0/2$. It is convenient to introduce the center-of-mass coordinate $\boldsymbol{R}\equiv(\boldsymbol{X}_1+\boldsymbol{X}_2)/2$ and the relative coordinate $\boldsymbol{r}\equiv\boldsymbol{X}_2-\boldsymbol{X}_1$.

For $p_1 q_1 = p_2 q_2$, we obtain

$$\boldsymbol{R} = -\frac{v_s t}{1+\tilde{\alpha}^2}\begin{pmatrix} 1 \\ p_1 q_1 \tilde{\alpha} \end{pmatrix}, \quad (3)$$

where $\tilde{\alpha}=\alpha D/G$. Thus, the center of mass of vortices flows in an oblique direction with velocity v_s. The transverse direction of the velocity depends on the sign of $p_1 q_1$ $(=p_2 q_2)$. The intervortex distance is given by

$$r = \sqrt{Y_0^2 + 2 q_1 q_2 \frac{\tilde{\alpha}}{1+\tilde{\alpha}^2}\frac{I}{G} t}. \quad (4)$$

For $q_1 q_2=-1$, due to the attractive force, r decreases with time, and the pair annihilation will occur with a shrinking spiral motion (note that polarities are opposite here, $p_1 p_2 = -1$). This explains the simulation result of Fig. 3. For the v-v (or $\bar{v}$-$\bar{v}$) pair with same polarity ($q_1 q_2=1$ and $p_1 p_2=1$), r increases with time.

For $p_1 q_1 = -p_2 q_2$, we solve Eq. (2) perturbatively in α $(\ll 1)$. The result up to $\mathcal{O}(\alpha)$ is given by

$$\boldsymbol{R} = -Vt\hat{x}, \quad (5)$$

$$\boldsymbol{r} = (Y_0 - 2 p_1 q_1 \tilde{\alpha} V t)\hat{y}, \quad (6)$$

where

$$V = v_s - p_1 q_2 \frac{I}{Y_0 G}. \quad (7)$$

Thus, the center of mass of two vortices flows along the wire. This direction depends both on the combinations of (p_1,q_1,p_2,q_2) and the relative magnitude between v_s and $I/(Y_0 G)$. When the mutual force I/Y_0 between the vortices exceeds the spin-transfer force Gv_s, the vortices move against the spin current [Figs. 5(b3), 5(b8), 5(c4), 5(c7)]. The numerical result for the rectilinear motion of the $v-\bar{v}$ pair with same polarity in Figs. 4(a)–4(g) corresponds to Fig. 5(c2). Dynamics of the two-vortex system is summarized in Fig. 5.[46]

The precise mechanism of the vortex-antivortex pair nucleation is yet to be investigated. Here, we present a scenario based on the fact that the spin current directly couples to the topological charge,

$$\frac{1}{2\pi}\int d^2x\boldsymbol{m}\cdot(\partial_x\boldsymbol{m}\times\partial_y\boldsymbol{m})=pq, \tag{8}$$

of the vortex configuration. As seen from the equation of motion [Eq. (2)],[15,21,29,30,45] a single vortex under spin current feels a force (potential gradient), $-pq\boldsymbol{G}\times\boldsymbol{V}_s$, analogous to a charged particle, with charge pq, in a fictitious electric field, $-\boldsymbol{G}\times\boldsymbol{V}_s$. In this picture, the pair nucleation may be viewed as the "ionization" of the originally "neutral" (uniformly magnetized) state into two "charged" objects whose topological charges are $pq=+1$ and -1, respectively.

IV. SUMMARY AND OUTLOOK

In this paper, we have demonstrated the important role of vortices in the magnetization dynamics of thin magnetic films and wires driven by large spin-polarized DC current based on micromagnetic simulations and analytical calculations. It includes pair creation, pair dynamics, and pair annihilation. In the case of individual annihilation through the sample edges, magnetic domain walls are created.

Dynamics of two interacting vortices was found to depend crucially on their vorticity and polarity. It was observed that pair creation and annihilation are such that vortex and antivortex created in pair in the bulk have the same polarity, whereas the pair annihilation is possible only between those with opposite polarity, despite topological obstruction.

The current required here for vortex nucleation in a uniform wire is of order of 10^{13} A/m^2. For application to memories where a bit of information is stored as the presence or the absence of a domain wall, lower current is favorable. This can be achieved, for instance, by introducing inhomogeneity such as notches, as shown in Fig. 6. In this case, the threshold for vortex nucleation is reduced at the edge of the notches to be about one-half, $j_s=5.6\times10^{12}$ A/m^2. Confined domain walls between notches would thus be useful for memories manipulated at low current.

[1] L. Berger, J. Appl. Phys. **71**, 2721 (1992).
[2] J. C. Slonczewski, J. Magn. Magn. Mater. **159**, L1 (1996).
[3] L. Berger, Phys. Rev. B **54**, 9353 (1996).
[4] M. Yamanouchi, D. Chiba, F. Matsukura, and H. Ohno, Nature (London) **428**, 539 (2004).
[5] M. Yamanouchi, D. Chiba, F. Matsukura, T. Dietl, and H. Ohno, Phys. Rev. Lett. **96**, 096601 (2006).
[6] E. Salhi and L. Berger, J. Appl. Phys. **73**, 6405 (1993).
[7] N. Vernier, D. A. Allwood, D. Atkinson, M. D. Cooke, and R. P. Cowburn, Europhys. Lett. **65**, 526 (2004).
[8] A. Yamaguchi, T. Ono, S. Nasu, K. Miyake, K. Mibu, and T. Shinjo, Phys. Rev. Lett. **92**, 077205 (2004).
[9] M. Kläui, P. O. Jubert, R. Allenspach, A. Bischof, J. A. C. Bland, G. Faini, U. Rüdiger, C. A. F. Vaz, L. Vila, and C. Vouille, Phys. Rev. Lett. **95**, 026601 (2005).
[10] G. S. D. Beach, C. Knutson, C. Nistor, M. Tsoi, and J. L. Erskine, Phys. Rev. Lett. **97**, 057203 (2006).
[11] M. Hayashi, L. Thomas, C. Rettner, R. Moriya, X. Jiang, and S. S. P. Parkin, Phys. Rev. Lett. **97**, 207205 (2006).
[12] G. Tatara and H. Kohno, Phys. Rev. Lett. **92**, 086601 (2004).
[13] A. Thiaville, Y. Nakatani, J. Miltat, and N. Vernier, J. Appl. Phys. **95**, 7049 (2004).
[14] S. Zhang and Z. Li, Phys. Rev. Lett. **93**, 127204 (2004).
[15] A. Thiaville, Y. Nakatani, J. Miltat, and Y. Suzuki, Europhys. Lett. **69**, 990 (2005).
[16] S. E. Barnes and S. Maekawa, Phys. Rev. Lett. **95**, 107204 (2005).
[17] Y. B. Bazaliy, B. A. Jones, and S. C. Zhang, Phys. Rev. B **57**, R3213 (1998).
[18] J. Fernández-Rossier, M. Braun, A. S. Núñez, and A. H. MacDonald, Phys. Rev. B **69**, 174412 (2004).
[19] Z. Li and S. Zhang, Phys. Rev. Lett. **92**, 207203 (2004).
[20] J. Shibata, G. Tatara, and H. Kohno, Phys. Rev. Lett. **94**, 076601 (2005).
[21] D. L. Huber, J. Appl. Phys. **53**, 1899 (1982).
[22] S. W. Yuan, H. N. Bertram, J. F. Smyth, and S. Schultz, IEEE Trans. Magn. **28**, 3171 (1992).
[23] K. S. Lee, B. W. Kang, Y. S. Yu, and S. K. Kim, Appl. Phys. Lett. **85**, 1568 (2004).
[24] M. Kläui, M. Laufenberg, L. Heyne, D. Backes, U. Rüdiger, C. A. F. Vaz, J. A. C. Bland, L. J. Heyderman, S. Cherifi, A. Locatelli, T. O. Mentes, and L. Aballe, Appl. Phys. Lett. **88**, 232507 (2006).
[25] Y. Togawa, T. Kimura, K. Harada, T. Akashi, T. Matsuda, A. Tonomura, and Y. Otani, Jpn. J. Appl. Phys., Part 2 **45**, L1322 (2006).
[26] T. Ishida, T. Kimura, and Y. Otani, Phys. Rev. B **74**, 014424 (2006).
[27] S. Kasai, Y. Nakatani, K. Kobayashi, H. Kohno, and T. Ono, Phys. Rev. Lett. **97**, 107204 (2006).
[28] K. Yamada, S. Kasai, Y. Nakatani, K. Kobayashi, H. Kohno, A. Thiaville, and T. Ono, Nat. Mater. **6**, 270 (2007).
[29] J. Shibata, Y. Nakatani, G. Tatara, H. Kohno, and Y. Otani, Phys. Rev. B **73**, 020403(R) (2006).
[30] J. He, Z. Li, and S. Zhang, Phys. Rev. B **73**, 184408 (2006).
[31] In general, another type of current-induced spin torque, $\beta\mathbf{m}\times(\boldsymbol{v}_s\cdot\nabla)\boldsymbol{m}$, appears on the right-hand side of Eq. (1), where β is a dimensionless constant of the order of 10^{-2}. For a special case of $\alpha=\beta$ (Refs. 16 and 43), the current-induced instability of the uniformly magnetized state disappears, implying that the vortex formation does not occur. (This is also confirmed by our simulations.) However, recent microscopic theory showed that $\alpha\neq\beta$, in general (Ref. 44). On this ground, we take $\beta=0$ in this paper for simplicity.
[32] Y. Nakatani, Y. Uesaka, and N. Hayashi, Jpn. J. Appl. Phys., Part 1 **28**, 2485 (1989).
[33] H. Fukushima, Y. Nakatani, and N. Hayashi, IEEE Trans. Magn. **MAG-34**, 193 (1998).
[34] N. Hayashi, K. Saito, and Y. Nakatani, Jpn. J. Appl. Phys., Part 1 **35**, 6065 (1996).
[35] Y. Nakatani, A. Thiaville, and J. Miltat, Nat. Mater. **2**, 521 (2003).

[36] W. F. Brown, Phys. Rev. **130**, 1677 (1963).
[37] Y. Nakatani, Y. Uesaka, N. Hayashi, and H. Fukushima, J. Magn. Magn. Mater. **168**, 347 (1997).
[38] K. S. Lee, S. Choi, and S. K. Kim, Appl. Phys. Lett. **87**, 192502 (2005).
[39] R. Hertel and C. M. Schneider, Phys. Rev. Lett. **97**, 177202 (2006).
[40] B. V. Waeyenberge, A. Puzic, H. Stoll, K. W. Chou, T. Tyliszczak, R. Hertel, M. Fähnle1, H. Brückl, K. Rott, G. Reiss, I. Neudecker, D. Weiss, C. H. Back, and G. Schütz, Nature (London) **444**, 461 (2006).
[41] O. A. Tretiakov and O. Tchernyshyov, Phys. Rev. B **75**, 012408 (2007).
[42] K. Y. Guslienko, X. F. Han, D. J. Keavney, R. Divan, and S. D. Bader, Phys. Rev. Lett. **96**, 067205 (2006).
[43] Y. Tserkovnyak, H. J. Skadsem, A. Brataas, and G. E. W. Bauer, Phys. Rev. B **74**, 144405 (2006).
[44] H. Kohno, G. Tatara, and J. Shibata, J. Phys. Soc. Jpn. **75**, 113706 (2006).
[45] A. A. Thiele, Phys. Rev. Lett. **30**, 230 (1973).
[46] If a finite β is taken into account (Ref. 30), the term $-\beta D\boldsymbol{v}_s$ is added on the left-hand side of Eq. (2). This term slightly tilts the direction of the vortex orbital motion. For $p_1q_1p_2q_2=1$, $\tilde{\alpha}$ in the parentheses in Eq. (3) is replaced by $\tilde{\alpha}(1-\beta/\alpha)$. Similarly, for $p_1q_1p_2q_2=-1$, $\tilde{\alpha}$ is replaced by $\tilde{\alpha}(1-\beta/\alpha)$ and the condition $v_s > I/Y_0G$ by $v_s(1-\beta/\alpha) > I/Y_0G$.